Accuracy of Registration of PET, SPECT and MR Images of a Brain Phantom

Timothy G. Turkington, Ronald J. Jaszczak, Charles A. Pelizzari, C. Craig Harris, James R. MacFall, John M. Hoffman and R. Edward Coleman

Department of Radiology, Duke University Medical Center, Durham, North Carolina; Department of Radiation Oncology, University of Chicago, Chicago, Illinois

Accuracy of a surface-fitting algorithm for three-dimensional image registration of single photon emission computed tomography (SPECT), positron emission tomography (PET), and magnetic resonance (MR) images was tested using a three-dimensional, water-fillable brain phantom. Multislice or volume image sets were acquired for each modality. Small fiducial markers were attached to assess accuracy of surface fitting and provide an alternate fitting technique. A maximum gradient technique was found to work well for SPECT and PET edge detection. Transformation parameters for translation, rotation and scaling were determined by surface fit to match each SPECT and PET scan with MR images. Using the markers, overall translation errors were found to be <2 mm in each direction and rotational errors <2 degrees in every case. Errors for specific internal regions were also determined to be <2 mm for most regions, with only a few fits resulting in errors >3 mm for some cortical regions. Results indicate surface fitting to be sufficiently accurate for visual comparison of registered images and for enhanced SPECT and PET region of interest (ROI) determination and image reconstruction.

J Nucl Med 1993; 34:1587–1594

Emission computed tomography (ECT) imaging, including PET and SPECT, provides functional information. Registration of ECT with high-resolution structural information such as obtained from MR images has many clinical and research uses. For example, whenever correlating information from multimodality, multislice studies performed on a patient, images from the different modalities should represent the same anatomy for optimal comparison. Matching slices can then be viewed side-by-side or superimposed with some color scheme. Three-dimensional display techniques have also been developed for displaying and comparing image information (*1–3*). In addition, when quantitative information is desired from a functional study for a particular anatomic region, for example, blood flow in a brain region as measured using ^{15}O-water PET, the boundary of the region can be defined in the higher-resolution MR image and applied to the matching functional study. Several schemes have been suggested for improving PET and SPECT image reconstruction based on the higher resolution boundary and region information available in MR images (*4–8*). A series of international workshops has been held to address the issues of multimodality imaging (*9*).

Different image sets acquired in the same subject using the same or different modalities may differ in scale (pixel size), orientation (angle), and position. For some organs, the shape may change relative to patient position. If the organ of interest is the brain, then the shape may be assumed constant.

Several methods of ensuring registration of multislice image sets have been described. A head holder can be used with or without fiducial markers that enforce repeatable positioning or allow image alignment based on the markers (*10–13*). Anatomic features alone can be used to align image sets (*14–16*). Use of anatomical features can be separated into techniques in which an expert identifies location of features common to the two image sets, and techniques in which organ surfaces are determined in the two image sets and matched through a minimization program that transforms one surface to match the other.

Registration techniques based on anatomical features have the advantage that no special preparation or equipment is needed at the time of image acquisition (e.g., no specific head holders or markers). The scanning process is simplified by this technique making retrospective registration possible. In addition, processing of the data for alignment of images using the surface-fitting technique does not require an operator with expert knowledge of organ features.

One inherent problem with the surface-fitting technique is that the error of a particular fit cannot be determined from the fit itself. Residual misfit determined in fitting one surface to another measures how well the surfaces fit together after transformation. It is a measure of noise and local continuous symmetries in the surfaces and error in the surfaces due to axial undersampling, as well as the registration accuracy. A difference in small structure resolution in the image surfaces and noise in the surfaces will

Received Sept. 28, 1992; revision accepted May 11, 1993.

For correspondence and reprints contact: Timothy Turkington, Ph.D., Nuclear Medicine/Radiology, Duke University Medical Center, Box 3949, Durham, NC 27710.

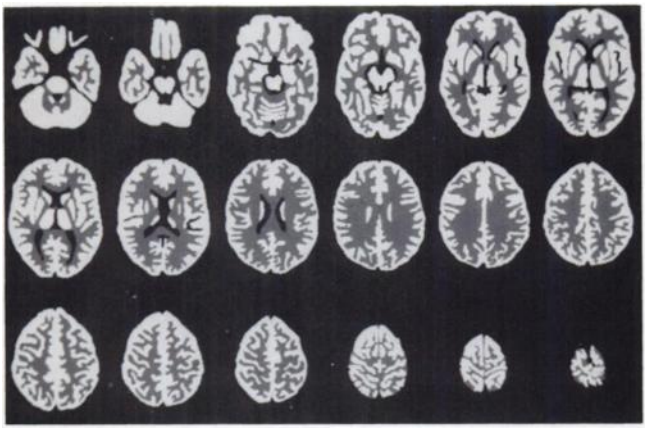

FIGURE 1. Images of phantom pattern. Gray matter has value of 4, white matter of 1, and ventricles 0.

FIGURE 2. Phantom with markers attached.

lead to a larger residual error even though an accurate transformation has been determined. Conversely, symmetry in the surfaces could give small residual errors that belie registration error. In an extreme example, spherical surfaces would fit well regardless of rotation angles.

Registration error may be defined as the difference in position of an anatomical point in one image set compared to its position in a second set that has been registered to the first. Surface-fitting registration error has been evaluated to varying degrees in several contexts (*16–19*). This study was performed to measure registration errors introduced by the surface-fitting technique when matching brain images from SPECT and PET images with MR brain images using the brain surface. It was also designed to assess contribution to the registration error from error in individual transformation parameters, i.e., to measure independently errors in rotational, translational and optional scaling parameters. To provide an ideal case in which underlying surface structures matched identically, a three-dimensional brain phantom was scanned using the three modalities, and the surface-fitting technique was applied. Markers attached to the outside of the phantom were used to measure error in the registration. Since quality of fit and therefore registration quality depend on surface definition, a different edge determination method was used which leads to improved surface matching and is much less operator-dependent.

METHODS

Phantom Description

The Hoffman three-dimensional Brain Phantom (*20*) (Data Spectrum, Inc., Hillsborough, NC) was used for this study. The phantom is a water-fillable cylinder containing 19 layers that are 6.4 mm thick. Each layer allows water to permeate various regions to match gray matter-to-white matter-to-ventricle ratio of 4:1:0, which is the approximate ratio of perfusion of these structures. A bitmap representation of the phantom is shown in Figure 1.

Ten plastic vials of inner diameter 6 mm and length 5 mm were attached to the outside of the phantom in two rings as shown in Figure 2. The markers were in the planes of the second and eighteenth phantom layers. This choice of marker size was based on the desire to have markers that were as small as possible and yet would still be measured in several slices in each modality. The cylindrical shape allowed easy attachment to the phantom and was indistinguishable from a spherical source for the lower resolution SPECT and PET studies. Since different vials were used for different modalities, paper dots 1 mm larger in diameter than the vials were taped to the phantom and covered with clear double-sided tape, to which the markers could be attached. This method allowed reattachment of the markers with an estimated error of less than 1 mm, based on the visibility of the dot edge around the marker base.

The phantom was filled with agents appropriate for each study. For MRI, the phantom and markers were filled with 0.16 *M* $CuSO_4$ solution. For SPECT, the phantom contained 30 mCi (1100 MBq) ^{99m}Tc solution and the markers each contained 20 μCi (0.7 MBq). For PET, the phantom was filled with 6 mCi (220 MBq) ^{18}F-2-fluoro-2 deoxyglucose (FDG) solution and the plastic vials, lined with copper tubing, were each filled with a piece of cotton containing ~3 μCi (0.11 MBq) FDG. Copper lining was inserted in the PET vials to guarantee annihilation of all the positrons within the vial.

Scan Parameters and Reconstruction

The MR scan was performed at 1.5 T (GE Signa, GE Medical Systems, Milwaukee, WI). The phantom was positioned in the scanner so that layers of the phantom were parallel to transaxial slices in the final images. A T1-weighted volume scan (TR = 18, TE = 9, flip angle = 60°) was performed with 2-mm slice thickness and 24-cm field of view, giving $(0.94\ mm)^2$ pixels in the final 256 × 256 images. Sixty slices were acquired and stored. Slices representing 18 layers are shown in Figure 3. The ratio of gray matter-to-white matter pixel values varied from slice to slice and ranged from 8:1 to 3:1 depending on how the MR slice was aligned with the phantom layers. Black spots in the white matter regions are artifacts resulting from air bubbles trapped in the phantom. Because layers of the phantom were large compared with MRI resolution, images produced with the phantom at other orientations in the scanner yielded discontinuities in edges and regions unsuitable for surface fitting.

The SPECT images were acquired on a three-headed scanner (Trionix Triad, Trionix Research Labs, Twinsburg, OH) with low-energy ultra-high-resolution collimators. The phantom was first scanned aligned with the camera axis of rotation and then at four

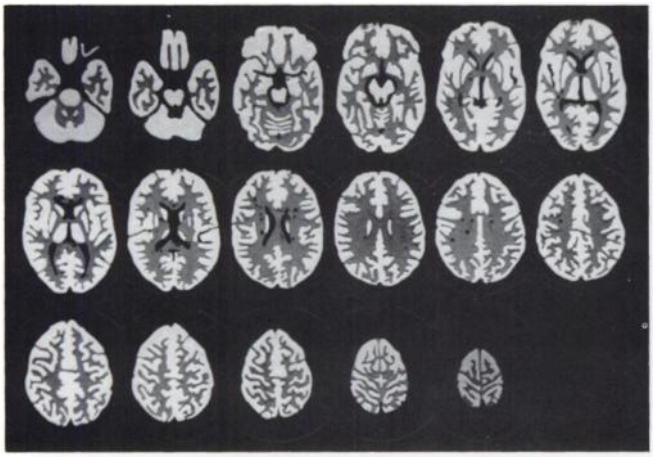

FIGURE 3. Unregistered MR images. Top markers are visible in two slices.

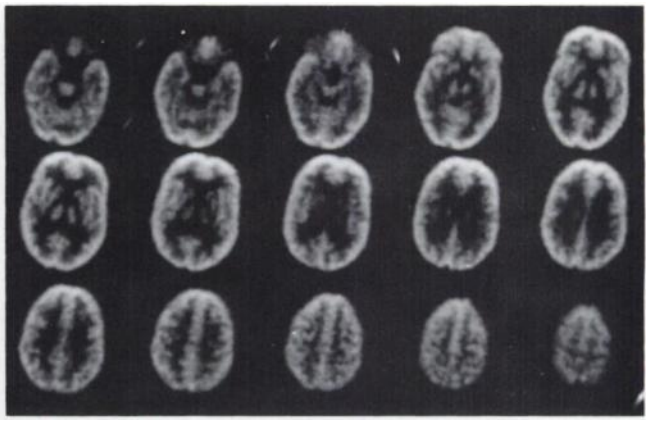

FIGURE 5. Unregistered PET images with no attenuation correction. Phantom is not aligned with central axis. Markers are visible in some slices.

different orientations relative to the scanner in which the phantom was tilted and turned to simulate or even exaggerate various angles at which a real head might rest on a head holder. In the fifth orientation, the phantom was positioned vertically, 90° away from the orientation aligned with the axis of rotation. Each scan was 13 min with 3° angular sampling, and activity at the scan times ranged from 20 to 30 mCi (740–1100 MBq) resulting in total counts (~30 *M*) that were approximately three times levels for our clinical studies, where a typical slice contains 200 K counts.

Transverse slices were reconstructed with filtered backprojection with a modified Hann filter with a cutoff frequency of 1.15 cm^{-1} and multiplicative attenuation correction. Pixel size for projections and reconstructed images was $(3.56\ mm)^2$. Final image sets consisted of 60 3.56-mm slices, each 128 × 128 pixels. Representative slices from one acquisition are shown in Figure 4. This combination of collimator and reconstruction filter frequently is used for human brain studies in our lab, and results in a resolution of approximately 11 mm (FWHM) for brain studies. The axial resolution was slightly better (~8 mm) since no smoothing was done axially.

The PET images were acquired on an eight-ring system (4096Plus, GE Medical Systems, Milwaukee, WI). The phantom was scanned at three different orientations in the scanner. Two table positions were required to image the entire phantom and markers for each orientation. An interleave mode (not normally used for our patient brain studies) was used to halve the axial sampling interval for better position determination of the markers. Each acquisition was 4 min, resulting in approximately 1 million counts per slice, half of the typical count level for an FDG brain study in our laboratory. A modified Hann filter with a cutoff of 2.5 cm^{-1} was used for filtered backprojection reconstruction. This resulted in transaxial resolution of approximately 7 mm FWHM and axial resolution of 6 mm FWHM. After the data from the interleave and two table positions were rearranged, the entire image set for each phantom orientation consisted of 42 slices separated by 3.25 mm, each slice consisting of 256 × 256 $(1.5\ mm)^2$ pixels. To maintain the relatively high signals from the markers, attenuation was not corrected. One acquisition is shown in Figure 5. Tangential elongation of the markers is an artifact of backprojecting when some projections are attenuated much more than others.

All image sets were transferred to one computer for registration via a common Ethernet link.

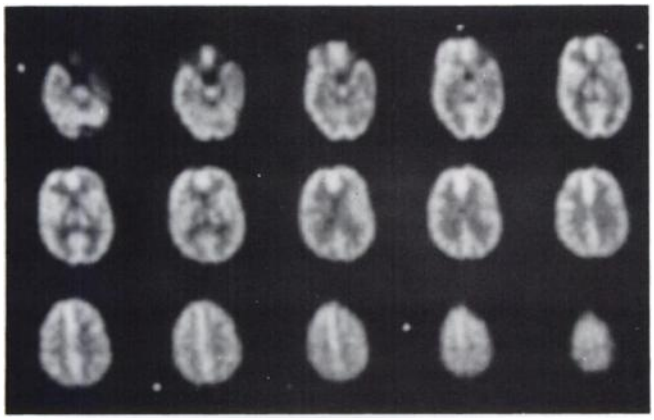

FIGURE 4. Unregistered SPECT images with attenuation correction. Phantom is not aligned with axis of rotation. Markers are visible in some slices.

Brain Edge Determination

The first step in the surface-fitting technique was to define brain edge boundaries on individual slices from each image set. This task was performed with our internally generated image display and analysis software "Specter" written for the X Window System. Different edge detection techniques were used, with a simple threshold technique sufficing for MRI and a more sophisticated method required for ECT.

For the MR scan, one image slice was used for each layer of the phantom. Each 6.4-mm phantom layer was contained in three or four of the 2-mm image slices and the middle slice of each group of three or four was chosen, leaving gaps of two or three unused slices. For each chosen slice, the outer edge of the brain was determined by inward searches along radial paths toward the image center. Paths started at each of the pixels on an ellipse drawn to surround the brain image and exclude the markers, when present. The edge for each radial path was defined to be the first pixel above a threshold of half the gray matter intensity, determined by drawing ROIs, and which was uniform (± 10%) throughout the slices. The resulting edge points were treated as vertices of a polygon. Duplicate points resulting from convergence of the inward radial paths were eliminated and some undesirable points resulting from nonanatomical support pieces in the phantom, as seen in Figure 6, were removed manually. The contour was then smoothed by adjusting the position of each point so that its dis-

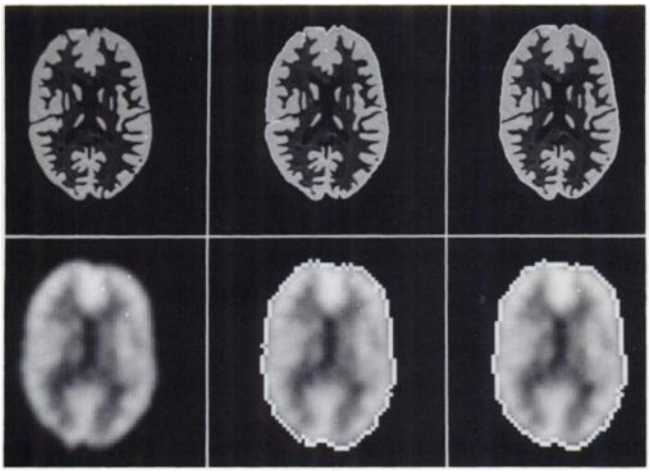

FIGURE 6. Edge determination. Upper images show edge determination for MR images: before edge detection, after threshold application and after smoothing and collinear point elimination. Lower images show process for SPECT: before edge detection, after first derivative maximum search and after smoothing and point elimination.

tance to the center was the mean of its neighbors' initial distances, and the number of points was reduced with two iterations of an algorithm eliminating any point that was within half a pixel of the line connecting its neighbors. Figure 6 shows results of the boundary determination for one MR slice. In the lowest slice where the temporal lobes and cerebellum are separate, the resulting contour included inward spikes between these regions.

Edge points for the SPECT and PET scans were also determined in inward radial searches, but with different criteria. A one-dimensional filter with kernel (−0.5, 0, 0.5) was applied to each inward path, yielding a smoothed first derivative. A threshold of approximately one-tenth the maximum pixel value was applied to the original image to suppress the backprojection streak effects and other noise, and the first pixel above this threshold which was also a local maximum in the first derivative was called the edge for that path. Redundant (collinear) points were removed from the list as they were for the MR boundaries, and radial smoothing was applied to the resulting polygon. Once this was done, the collinear-point removal described for MR boundaries was applied once. Figure 6 shows results of the boundary determination for one SPECT slice. Boundaries were not determined in the lowest slices where the cerebellum and temporal lobes are separated.

Motivation for using the maximum in the first derivative as opposed to a simple threshold came from difficulty in determining an appropriate threshold. Regions in the cerebral cortex that are thin yield lower peak pixel values due to resolution effects, and in actual patient studies, brain defects may result in lowered regional uptake, prohibiting a common threshold method. The first derivative maximum edge criterion is valid if the system response kernel has a peak (slope of zero) at $x = 0$, as would be the case for any symmetric point spread function, provided the anatomic regions are large compared to system resolution, a condition that may not hold for thin parts of the cerebral cortex. For this study, routinely performed attenuation correction was not performed on PET images. The resulting intensity variation around the cerebral cortex provided a good test for edge detection.

Boundaries were determined for every second slice, resulting in 7.12-mm spacing in SPECT and 6.5-mm spacing in PET, and covered the region from the top of the brain to the lowest slice of completely contiguous brain. Using every other slice from PET corresponded to omitting the interleave, so that the surface fitting was based on the normally used (noninterleaved) slice spacing. Surface information (the collection of slice boundaries) from each image set was put into a "head" file (for the MR scan) or "hat" file (for the SPECT and PET scans) (*16*). These contained the coordinates (x, y, z) of all edge points determined for the scan.

Surface Fitting

Once surfaces were determined, the program SurfaceFit (*16*) was used to match each PET and SPECT surface to the MR surface. Input to the program consisted of the MR "head" file and a "hat" file from PET or SPECT, as well as information concerning pixel sizes and slice separations. The program uses a nonlinear least-squares technique to find a coordinate transformation which minimizes the distances of the points in the "hat" file to the surface defined by the contours in the "head" file. This transformation includes translation (in all three dimensions), rotations (three parameters), and scaling (in three dimensions).

The initial parameters for the fitting procedure were the defaults used by the SurfaceFit program. The relative translation between the surfaces is set such that centroids of the edge points for the two sets are aligned. Angles simply come from the initial scan planes, so that original slice planes from the two scans are aligned. The scale parameters are set to 1.0, meaning the initial relative scale between the two surfaces is set to the known pixel size ratio.

Since the program considers the different image pixel sizes before beginning the fit, the optional scaling done by SurfaceFit corrects for inaccuracies in the pixel size values as well as inconsistencies in the boundary detection process. To evaluate the effect of the optional scaling, all fits were done with and without the three scaling parameters included in the fit. When scales were not allowed to change by program, they were set to 1.0, meaning that known pixel size ratio provided the scale.

Position Measurement, Error Determination

Positions of the ten markers were measured in all original image sets. For the MR image, a marker's position was determined by first drawing a small ROI around the marker in the central slice containing the marker. Most markers were visible in five MR slices. Then, a three-dimensional pixel-weighted centroid was calculated over all pixels in the ROI and over all slices containing the marker:

$$C = \frac{\sum_i I_i r_i}{\sum_i I_i},$$

where i is an index over all pixels in the multislice ROI, I_i is the direct MR value of pixel i, r_i is the position of pixel i, and C is the three-dimensional centroid. The result was a point in the image coordinates representing the center of the marker. This point was calculated for all ten markers.

For SPECT and PET images, the marker locations were determined in all dimensions by a fitting process. First, a rectangular region was drawn around the marker in the slice containing the most counts for the marker. Then, for the x-position, a parabola was analytically fit to count sums from the five y-z planes within the region that contained the most counts and the peak of the parabola was considered to be the marker center position. The y

and z values were determined similarly except only three x-y planes were used for the z measurement. This method has been shown to agree closely (<1 mm) with a centroid calculation when the marker is isolated (*19*) and has the advantage that surrounding activity has less effect since the calculation is based only on a 5 × 5 × 3 voxel volume. It is also an improvement over simply picking the most intense pixel as the center. The choice of a parabolic shape was based on ease of implementation and reasonable fit to data in all three dimensions.

RESULTS

The fitting procedure converged in approximately 1 min (Sun SPARCstation II), and only in one case (the fifth SPECT acquisition in which the phantom was oriented vertically in the scanner, 90° from the MR orientation) did the program require operator intervention. Table 1 shows residual (the square root of the mean squared distance of the ECT points from the MR surface) for each fit as well as the scale parameters determined when scaling was allowed to vary. Residuals are larger for SPECT fits than PET when the scale was allowed to vary, due to the coarser sampling. The mean scale factors obtained are 0.977 for SPECT and 0.973 for PET. These factors, although consistently <1.0, represent a small error in the surface determination. For an edge 5 cm from the brain center, a scale of 0.975 represents an error of 1.25 mm, which is much less than one SPECT or PET pixel.

Table 2 shows the angles determined from both scaled and nonscaled fits. For rotation about the y- and z-axes, fits differ by more than 1.1° in only one case, and for rotation about the x-axis the worst difference is 2.2°, with the others less than 1.2°. In general, the nonunity scale factors could represent weakness in surface definition or error in assumed pixel sizes, or both. One strength of the surface-fitting technique is that it can be performed retrospectively with minimal knowledge of parameters related to the image sets (e.g., use of images digitized from films obtained from another institution). To measure errors in the worst case in which scaling is required because the exact pixel sizes are not known, all following results use the scaled fit parameters in transforming points from one scan frame to another.

To evaluate error in surface fitting, the marker positions measured in PET and SPECT scans were transformed to

TABLE 1
Residual Errors for Surface Fits for Fixed and Scaled Case

ECT Scan	Residual with scaling (mm)	Residual without scaling (mm)	Scaling factors		
			x	y	z
SPECT 1	1.9	2.5	0.97	0.98	0.98
SPECT 2	2.0	2.6	0.98	0.97	0.96
SPECT 3	1.9	2.5	0.96	0.99	0.98
SPECT 4	1.9	2.4	0.97	0.98	0.99
SPECT 5	2.4	2.9	0.97	0.98	0.99
PET 1	1.5	2.7	0.97	0.97	1.00
PET 2	1.5	2.7	0.97	0.96	0.97
PET 3	1.5	2.6	0.97	0.97	0.98

TABLE 2
Angle Determination Comparison with and without Scaling

ECT scan		Angle determination from fit (degrees)		
		θz	θy	θx
SPECT 1	Fixed	4.0	−1.9	0.6
	Scaled	4.5	−1.0	1.7
SPECT 2	Fixed	−3.7	−7.8	−5.8
	Scaled	−4.2	−8.0	−7.6
SPECT 3	Fixed	0.3	−7.2	−5.0
	Scaled	0.1	−6.7	−6.1
SPECT 4	Fixed	−5.6	−25.1	1.9
	Scaled	−5.6	−24.0	2.5
SPECT 5	Fixed	3.0	−0.1	−87.8
	Scaled	3.7	0.2	−88.1
PET 1	Fixed	2.3	1.9	0.5
	Scaled	2.3	1.9	0.6
PET 2	Fixed	−2.3	−3.5	0.8
	Scaled	−1.3	−3.1	0.6
PET 3	Fixed	11.1	−0.1	−7.4
	Scaled	10.6	0.8	−8.2

MR scan coordinates via the transformation determined from the surface fit. Positions were then compared to the positions measured from the MR scan itself. Differences between the positions for one PET scan compared with MR are shown in Table 3. Errors include the marker relocation error between scans and the marker position determination error as well as errors due to misregistration. Note that location of the markers far outside the actual brain region (~12 cm from the center) means that errors in transformation angle and scale affect position errors much more than locations inside the brain would be affected. An x-angle error of one degree, for example, would lead to position error of (100 mm) sin (1°) = 2 mm in the absence of any translation fit error, and a scaling value of 0.97 in the x-dimension would contribute 0.03 × 100 mm = 3 mm error for the marker x position.

Table 4 shows the mean and root-mean-square (RMS) error for eight markers for each ECT scan compared to an MR scan. The error is simply the difference between positions measured in the MR scan and the transformed positions measured in the ECT scans. The eight markers chosen formed a symmetric box around the center of the phantom. The mean error is the error expected at the middle of the brain, or the error in the translation parameters, since finding the mean of the outer markers reduces or cancels errors in fit angle and scale because the eight markers were symmetrically distributed. In addition, using the mean reduces the effect of the marker position determination error, assuming these errors were not correlated. The RMS values reflect all sources of error and include the effects of marker relocation error, measurement error and misregistration (enhanced by distance of markers from the phantom center). We therefore conclude that errors in the translational component of the fitting (and therefore errors for points near the middle of the brain) were less than 2.0 mm for SPECT and less than 1.3 mm for PET.

TABLE 3
Marker Position Difference for One PET Scan Transformed to MR Frame

Marker	Difference in marker positions (mm)		
	x	y	z
1	2.9	−4.2	−3.1
2	2.6	−0.5	0.3
3	−1.7	−0.1	2.5
4	−2.4	−2.0	2.4
5	−1.3	−4.6	−0.2
6	1.9	−0.3	−3.9
7	−0.3	1.5	−0.7
8	−1.7	1.5	−0.2
9	−3.6	−0.5	0.1
10	−3.4	0.7	−2.0

To evaluate the effect of fit-angle error, a separate fit was done for each ECT scan to the MR scan using the markers. This was also done with SurfaceFit using a feature in which multiple objects can be transformed together. This fitting was done without scaling. The differences between the angles determined from the marker fit and the angles determined from the surface fit are shown in Table 4. In all cases, error in rotation about the y- and z-axes is less than 1.5°, with an RMS value of 0.8°, and rotation error around the x-axis is less than 2.0°, with an RMS value of 1.3°.

An additional result of fits based on markers was an estimate of the combined errors of marker position measurements from images and repositioning of the markers on the phantom for different modalities. After ECT marker positions were fit to MR marker positions with no scaling, residual error for the ten-marker fit was 1.3–1.5 mm for the five SPECT to MR registrations and 1.6–2.1 mm for the three PET to MR registrations. These values represent RMS position errors for markers in all three dimensions, including measurement error in the MR images, measurement error in the ECT images, and error in repositioning markers. The higher errors for PET could be due to difference in centroids of positron annihilations in copper inserts, as compared to centroids of filled solutions for MRI and SPECT. With these small errors in marker position determination, the overall accuracy in fitting six parameters (three translational and three rotational) with ten markers (each with three coordinates) was assumed to be sufficiently accurate to provide a reference for the surface fitting.

Since translation, rotational, and scaling parameter errors are clearly coupled, registration error for a specific point in the brain is not easily estimated. We identified points in eight brain regions on the MR study, transformed these to each of the ECT studies using parameters based on marker fit (assumed to be accurate), and then transformed back using parameters from the scaled surface fits. Absolute position differences (e.g., $|x_{orig} - x_{trans}|$) were measured between the originally selected points and the doubly transformed points to yield registration errors for each location for each ECT study. Results are summarized in Table 5 as mean absolute error and maximum absolute error over all eight studies for the eight regions.

DISCUSSION

The required accuracy of image registration depends on the particular application. In the case of the surface fit registration, this error is directly related to error in transformation parameters, since error at any point of interest may be calculated once error in the transformation parameters is known. For viewing matching slices from different modalities, error in the axial direction should not be greater than the slice-to-slice separation (to ensure the closest slice is used) and error within the slice plane is not important unless pixel-to-pixel comparison is done. For other purposes, such as using MR boundary or region information to improve ROI definition or to aid reconstruction, accuracy in all dimensions is important and should be much better than resolution of the lower resolution device if resolution restoration is expected.

Previous studies have shown various levels of accuracy in the surface-fitting technique. In one study (*16*), landmarks inside a skull phantom were compared after one set had been reformatted to match the other. MRI, CT, and transmission images acquired on a PET system were used for this study, with registration based on the outer head surface. Each modality was registered with each of the others. Two-dimensional centroids of structures in the phantom were compared in one image set versus another image set that had been resliced to match the first. When

TABLE 4
Registration Errors Measured from Marker Positions

ECT scan	Mean error (mm)			RMS error (mm)			Rotational error (degrees)		
	x	y	z	x	y	z	θz	θy	θx
SPECT 1	−0.3	−0.8	0.0	4.1	2.0	2.7	0.3	0.0	2.0
SPECT 2	−0.9	−1.9	0.3	3.1	2.2	2.4	0.2	0.9	0.0
SPECT 3	−1.2	−0.9	−1.1	4.6	2.7	3.9	−1.4	−1.5	1.7
SPECT 4	−0.6	−1.7	−0.4	3.4	2.5	2.2	0.8	1.5	0.8
SPECT 5	−0.5	−0.6	−0.2	4.3	1.9	1.8	1.2	−1.0	0.8
PET 1	−0.4	−1.2	−1.0	2.5	2.4	2.2	0.5	0.6	1.5
PET 2	−0.3	−0.8	−0.3	2.0	2.1	2.2	−0.4	0.4	1.4
PET 3	0.3	−0.9	−0.8	1.9	2.6	2.1	−0.2	0.4	1.5

TABLE 5
Registration Errors for Specific Regions in Brain Phantom. Mean and Maximum Absolute Deviations are Over the Eight Registered Sets.

	Mean deviation (mm)			Maximum deviation (mm)		
	x	y	z	x	y	z
Head of caudate left	0.7	1.0	0.4	1.1	1.3	0.9
Head of caudate right	0.3	1.0	0.4	0.5	1.6	0.9
Dentate nucleus right	0.9	1.1	0.9	2.4	2.1	1.5
Visual cortex	0.8	3.4	0.8	2.1	4.5	1.3
Sensory motor strip left	2.0	0.7	0.2	3.1	1.7	0.3
Sensory motor strip right	0.9	0.7	0.5	1.9	1.8	1.0
Ocular muscle left	0.9	1.1	0.9	2.4	2.1	1.5
Ocular muscle right	0.8	1.3	0.7	2.2	2.5	1.4

the MR image and resliced PET were compared, an RMS difference of 2.48 mm was measured for internal marks.

Another study (*17*) compared the position of the thalami in registered SPECT and MR images. Shifts in the location of the thalami were considerably larger than the SPECT pixel size of 1.67 mm, although contribution to error from position measurement was not considered. Another study compared two methods of PET-MRI registration, with the methods showing agreement but with no measurement of overall errors (*18*). The surface-fitting method has been shown to be accurate for realignment of serial SPECT scans (*19*).

This investigation was unique in several ways. First, both SPECT and PET results were obtained for multiple data sets. In contrast to a previous study (*16*), brain surface (emission) was used instead of head surface (transmission), the three-dimensional accuracy was measured and errors in the transformation parameters themselves were determined. Similarly, another study (*17*) was not sensitive to rotational error since the object measured was near the center of the brain, and quoted errors included error in measuring the thalamus position so the high level of accuracy of registration could not be isolated. Finally, our study incorporated ECT brain surface detection based on first-derivative maxima instead of a simple threshold technique.

Results show that the surface-fitting method works well on the brain phantom surface when matching SPECT and PET images to MR images. Accuracy requirements are task-dependent, but for simply finding matching slices and setting ROIs on MR images and applying to ECT for quantitative analysis, mismatches of 2 mm are reasonable and much smaller than the inherent resolution of the SPECT and PET systems.

Table 4 demonstrates that rotations about the x-axis were fit the worst. This greater error is explained by the high degree of symmetry of brain surface under rotations within a sagittal plane, particularly when lower structures of the brain are not considered. The range in error in this parameter is 0.0 to 2.0 degrees, resulting in errors up to (50 mm)*sin(2.0°) = 1.7 mm for points 5 cm from the brain center. The effect is somewhat larger than the x and y mean (translational) errors in Table 4 and will dominate even more for points further away from the center. We conclude, then, that rotational fitting, particularly around the x-axis, is the prevalent source of error for points away from the x-axis.

Table 5 shows more directly the errors that surface fitting introduced for specific brain regions. Centrally located heads of the caudate nuclei had errors of 1.6 mm or less in every case, with regions further from the center still showing average deviations less than 2 mm and maximum deviations less than 3.1 mm. The exception is in the y component error in the visual cortex region, likely due to the ~0.97 scaling since the region is far from the brain center in the y direction. This would justify nonscaled surface fitting when the pixel sizes are well known and high accuracy is required for regions far from the brain center.

Investigation of image registration using phantom imaging has several advantages that must be considered before applying these results to image registration of patient studies. First of all, boundary determination is simpler in the case with the phantom since with the phantom there is no activity outside the brain surface. In addition, with the phantom the underlying brain surfaces are known to be identical, whereas the human brain edges identified in MR may not correspond exactly to boundaries over which functional information changes. Finally, since brains are not identical in shape and since accuracy of the method certainly depends on the surface being fit (a more symmetric, sphere-like surface being more difficult to fit correctly), the accuracy may vary on a subject-to-subject basis.

Differences between phantom acquisition and processing parameters and those used for patients were kept to a minimum. Even though the interleave mode was used for PET acquisitions to improve the marker position measurement, only half of the resulting slices were used for the surface fit, resulting in the standard 6.5-mm slice spacing. The count densities were higher than patient studies for SPECT and lower for PET, with good results in both cases. We can conclude that count density was not a limiting factor, at least for these densities. Because of the stated differences (advantages and disadvantages) of the phantom imaging compared to patient imaging, we stress that additional investigation using humans is necessary to fully evaluate accuracy of this technique.

The ECT boundary determination method gave good

results. Because little scaling was required to match the resulting surfaces with MR surfaces, the maximum derivative edge criterion is appropriate in this model. This criterion also would allow for varying amounts of uptake and the apparent lower uptake in thinner parts of the cerebral cortex, as opposed to using a constant fixed threshold. Good edge point determination should allow good fitting with fewer points, which includes the possibility of ignoring edge points from regions of the brain whose function is abnormal. For this study the PET images were not corrected for attenuation, resulting in increased nonuniformity around the cortical regions. The success of the edge detection on these images (and success on the attenuation-corrected SPECT images with very similar scaling factors to match the MR images) supports a conclusion that this algorithm is robust under many conditions.

This technique of using the brain edge for surface fitting is currently limited to ECT blood flow and metabolism studies due to the necessity of defining the brain edge. ECT studies that do not result in localization of radioactivity in the gray matter, such as studies of blood-brain barrier permeability, could not be registered using this technique. However, SPECT and PET transmission scans or use of scattered radiation may be suitable for registration with the anatomic information from MRI in ECT studies without gray matter localization, but further studies are required to determine accuracy of these techniques.

ACKNOWLEDGMENTS

The authors thank Kim Greer, Sharon Hamblen, David Coates, and Thomas Hawk for their assistance in acquiring the data. Research was supported by DOE grant DE-FG05-91ER60894 and in part by DOE grant DE-FG05-90ER75577, NIH grants R01-CA33541 and R01-CA54092, and PHS grant S10-RR04176.

REFERENCES

1. Levin DN, Hu X, Tan KK, et al. The brain: integrated three-dimensional display of MR and PET images. *Radiology* 1989;172:783–789.
2. Valentino DJ, Mazziotta JC, Huang HK. Volume rendering of multimodal images: application to MRI and PET imaging of the human brain. *IEEE Trans Med Imaging* 1991;10:554–562.
3. Evans AC, Marrett S, Torrescorzo J, Ku S, Collins L. MRI-PET correlation in three dimensions using a volume-of-interest (VOI) atlas. *J Cereb Blood Flow Metab* 1991;11:A69–A78.
4. Chen C-T, Ouyang X, Wong W, Hu X, Johnson V, Ordonez C, Metz CE. Sensor fusion in image reconstruction. *IEEE Trans Nucl Sci* 1991;38:687–692.
5. Leahy R, Yan X. Incorporation of anatomical MR data for improved functional imaging with PET. In: Colchester ACF, Hawkes DJ, eds. *Information processing in medical imaging, 12th international conference.* Berlin: Springer-Verlag, 1991;105–120.
6. Llacer J, Veklerov E, Nunez J. Preliminary examination of the use of case specific medical information as "prior" in Bayesian reconstruction. In: Colchester ACF, Hawkes DJ, eds. *Information processing in medical imaging, 12th international conference.* Berlin: Springer-Verlag; 1991;81–93.
7. Gindi G, Lee M, Rangarajan A, Zubal IG. Bayesian reconstruction of functional images using registered anatomical images as priors. In: Colchester ACF, Hawkes DJ, eds. *Information processing in medical imaging, 12th international conference.* Berlin: Springer-Verlag; 1991;121–131.
8. Müller-Gärter HW, Links JM, Prince JL, et al. Measurement of radiotracer concentration in brain gray matter using positron emission tomography: MRI-based correction for partial volume effects. *J Cereb Blood Flow Metab* 1992;12:571–583.
9. Mazziotta JC, Koslow SH. Assessment of goals and obstacles in data acquisition and analysis from emission tomography: report of a series of international workshops. *J Cereb Blood Flow Metab* 1987;7:S1–S31.
10. Miuri S, Kanno I, Iida H, et al. Anatomical adjustments in brain positron emission tomography using CT images. *J Comput Assist Tomogr* 1988;12:363–367.
11. Vogl G, Schwer C, Jauch M, Wiethölter H, Kindermann U, Müller-Schauenburg W. A simple superposition method for anatomical adjustments of CT and SPECT images. *J Comput Assist Tomogr* 1989;13:929–931.
12. Meltzer CC, Bryan RN, Holcomb HH, et al. Anatomical localization for PET using MR imaging. *J Comput Assist Tomogr* 1990;14:418–426.
13. Evans AC, Beil C, Marrett S, Thompson CJ, Hakim A. Anatomical-functional correlation using an adjustable MRI-based region of interest atlas with positron emission tomography. *J Cereb Blood Flow Metab* 1988;8:513–530.
14. Kapouleas I, Alavi A, Alves WM, Gur RE, Weiss DW. Registration of three-dimensional MR and PET of the human brain without markers. *Radiology* 1991;181:731–739.
15. Evans AC, Marret S, Collins L, Peters TM. Anatomical-correlative analysis of the human brain using three-dimensional imaging systems. *Proc Soc Photo-Optical Instrumentation Engineers* 1989;1092:264–274.
16. Pelizzari CA, Chen GTY, Spelbring DR, Weichselbaum RR, Chen CT. Accurate three-dimensional registration of CT, PET, and/or MR images of the brain. *J Comput Assist Tomogr* 1989;13:20–26.
17. Pelizzari CA, Evans AC, Neelin P, Chen CT, Marrett S. Comparison of two methods for 3D registration of PET and MRI images. *Proceedings of the annual international conference of the IEEE Engineering in Medicine and Biology Society*. 1991;13:221–223.
18. Holman BL, Zimmerman RE, Johnson KA, et al. Computer-assisted superimposition of magnetic resonance and high-resolution technetium-99m-HMPAO and thallium-201 SPECT images of the brain. *J Nucl Med* 1990;32:1478–1484.
19. Turkington TG, Jaszczak RJ, Greer KL, Coleman RE, Pelizzari CA. Correlation of SPECT images of a three-dimensional brain phantom using a surface fitting technique. *IEEE Trans Nucl Sci* 1992;39:1460–1463.
20. Hoffman EJ, Cutler PD, Digby WM, Mazziotta JC. 3-D phantom to simulate cerebral blood flow and metabolic images for PET. *IEEE Trans Nucl Sci* 1990;NS-37:616–620.